Dynamics, Control and Simulation of a Mobile Robotic System for 6-DOF Motion Emulation

Xiaoli Bai, Jeremy Davis, James Doebbler, James D.Turner and John L.Junkins*

Abstract—**We are developing an autonomous mobile robotic system to emulate six degree of freedom relative spacecraft motion during proximity operations. A mobile omni-directional base robot provides x, y, and yaw planar motion with moderate accuracy through six independently driven motors. With a six degree of freedom micro-positioning Stewart platform on top of the moving base, six degree of freedom spacecraft motion can be emulated with high accuracy. This paper presents our approach to dynamic modeling, control, and simulation for the overall system. Compared with other simulations that introduced significant simplifications, we believe that our rigorous modeling approach is crucial for the high fidelity hardware in-the-loop emulation.**

Keywords: Dynamic Modeling, Non-Linear Control, System Simulation

1 Introduction

We are developing an autonomous mobile robotic system to emulate six degree of freedom (DOF) relative spacecraft motion during proximity operations [1], [2], [3]. The base uses an active split offset castor (ASOC) drive train to achieve omni-directional planar motion with target tracking position errors in the $\pm 1cm$ range and heading angle error in the $\pm 0.5^\circ$ range. With six independently controlled wheels, we achieve a nominally uniform motor torque distribution and reduce the total disturbances with system control redundancy. A CAD design of our one-third scale model prototype is shown in Fig. 1.

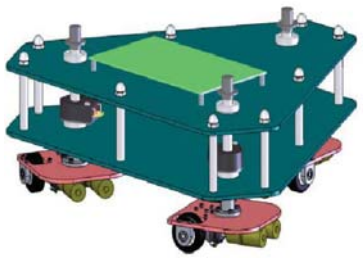

Figure 1: Base robot prototype

A micro-positioning Stewart platform is mounted on the moving base, as shown in Fig. 2. For the Stewart platform, the base plate and top plate are connected by six extensible legs; the parallel nature provides higher stiffness, higher loading capacities, and higher frequency compared with typical serial positioning devices. A complete dynamic model and a robust adaptive controller for the Stewart platform have been developed using a novel automatic differentiation method in [4]and[5]. The novel modeling approach makes it easy to modify the model assumptions and eliminates complicated derivative calculations. The robust adaptive control law guarantees that the tracking errors are asymptotically stable under even large parameter errors and slow-changing or constant external disturbances.

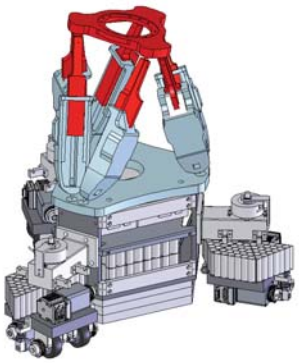

Figure 2: Stewart platform on the base

This paper focuses on modeling and control issues for the mobile base as well as the overall system simulation. Section 2 presents a dynamic model for the moving base robot with non-holonomic constraints using the Lagrangian approach through symbolic manipulation. Two methodologies for the control of the base are compared. One uses an input-output feedback to design a dynamic control law and another uses a kinematic control method. In Section 3, overall system simulation approach is described. Conclusions are presented in Section 4.

*The authors are with the Department of Aerospace Engineering, Texas A&M University, College Station, TX 77843 (email: xiaolibai@tamu.edu; jeremy.davis@tamu.edu; james.doebbler@tamu.edu; turner@aeromail.tamu.edu; junkins@tamu.edu)

2 Dynamics and Control for the Moving Base

Using ASOCs to provide true omni-directional mobility was introduced by H.Yu [6]. While kinematics and implementation have been discussed in [6], no dynamic models have been studied for mobile robots driven by ASOCs. In fact, there have been many papers written about solving the problem of dynamic model formulation under non-holonomic constraints using the kinematic model, but only a few papers addressing the integration of the non-holonomic kinematic controller with the dynamics of the mobile robot [7]. "Perfect velocity tracking" is always assumed in the available papers, which may not be the truth in reality [8]. This paper formulates a rigorous approach to track the reference path while taking account of the system dynamics. The mobile base can achieve true omni-directional motion without wheel reorientation, and also achieve higher precision control with higher loading capacity compared with the model discussed in [7], [8], [9]. Furthermore, our modeling and control approaches are very general and applicable to a significant class of similar systems.

2.1 Kinematic Analysis

A top view representation of the entire base assembly with the frame definitions is shown in Fig. 3. The three vertex points of the triangular base are all pivot points, each of which is connected to a castor, and the castor is connected to two wheels through shafts. Each castor is free to rotate about its pivot point and each wheel is independently driven by a mounted motor.
Kinematic equations are derived as follows. Knowing the velocity of the mass center of the triangular base together with the castor angles, and utilizing non-slippage constraints for the six wheels (the wheels roll without slip and also can not have side slip), the velocity of each wheel and shaft is uniquely defined. The velocity of the triangular base includes its translational velocity $\mathbf{v}_b = [\dot{x}, \dot{y}, 0]^T$ and rotational velocity $\dot{\psi}$ about its center of mass, where ψ is the rotational angle between the inertial frame and the base body frame.
The velocity of the i^{th} pivot point is computed by

$$\mathbf{v}_{p_i} = \mathbf{v}_b + \mathbf{BI}[-\dot{\psi}Rsin(\phi_i), \dot{\psi}Rcos(\phi_i), 0]^T \qquad (1)$$

where

$$\mathbf{BI} = \begin{bmatrix} \cos(\psi) & -\sin(\psi) & 0 \\ \sin(\psi) & \cos(\psi) & 0 \\ 0 & 0 & 1 \end{bmatrix} \qquad (2)$$

and ϕ is the angle between $\hat{\boldsymbol{b}}_1$ and the line connecting base center of mass to the i^{th} pivot point, and for the symmetric base, $\phi_1 = 0°$, $\phi_2 = 120°$, and $\phi_3 = 240°$; **BI** is the direction cosine matrix that transforms components of a vector in the **B** frame $\{\hat{\boldsymbol{b}}_1, \hat{\boldsymbol{b}}_2, \hat{\boldsymbol{b}}_3\}$ to the same vector with components in the inertial frame; R is the distance from the base center of the mass to the pivot point. The

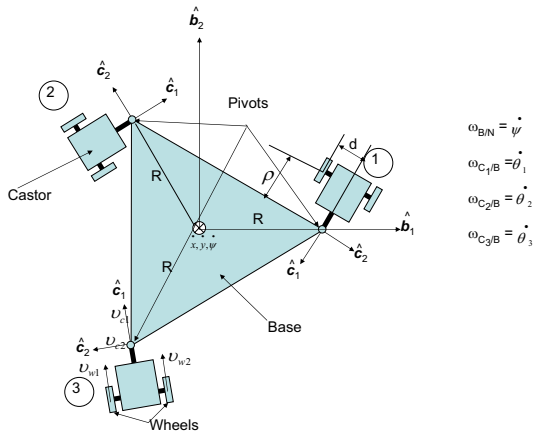

Figure 3: Top view of the base

inertial velocity of this pivot point is expressed in the castor **C** frame $\{\hat{\boldsymbol{c}}_1, \hat{\boldsymbol{c}}_2, \hat{\boldsymbol{c}}_3\}$ as $\mathbf{v}_{c_i} = [v_{c_1}, v_{c_2}, 0]$ using

$$\mathbf{v}_{c_i} = \mathbf{IC}\mathbf{v}_{p_i} \qquad (3)$$

where

$$\mathbf{IC} = \begin{bmatrix} \cos(\psi + \theta_i) & \sin(\psi + \theta_i) & 0 \\ -\sin(\psi + \theta_i) & \cos(\psi + \theta_i) & 0 \\ 0 & 0 & 1 \end{bmatrix} \qquad (4)$$

and θ_i is the rotational angle between the i^{th} castor **C** frame and the base **B** frame. Angular velocity of the castor with respect to the inertial frame is

$$\omega_i = \dot{\theta}_i + \dot{\psi} \qquad (5)$$

Using the no side slip constraints, this velocity can also be expressed as

$$\tilde{\omega}_i = v_{c_2}/\rho; \qquad (6)$$

and the velocities of the two wheels are

$$v_{w_1} = v_{c_1} - d\omega_i \qquad (7)$$

$$v_{w_2} = v_{c_1} + d\omega_i \qquad (8)$$

The velocities of the shafts are solved for in the same way. As shown in Fig. 3, ρ is the distance from the pivot point to the center of the wheels along $\hat{\boldsymbol{c}}_1$ direction and d is the same distance along $\hat{\boldsymbol{c}}_2$ direction.

2.2 Dynamic Equations

For the mobile base, the system energy includes the kinetic energy of the triangular base, three castors, six shafts and six wheels. Since we ignore the vertical motions in this paper, no potential energy is involved. The same approach developed below will be used in the future to derive a three dimensional model, which

includes the potential energy change because of the floor irregularities.

Twelve generalized coordinates $\boldsymbol{q} = [x, y, \psi, \theta_1, \theta_2, \theta_3, \Pi_1, \Pi_2, \Pi_3, \Pi_4, \Pi_5, \Pi_6]^T$ are chosen for the base system, which includes two translational and one angular position of the triangular base, three angular positions of the castors, and six angular positions of the wheels, respectively. The corresponding twelve generalized velocities are not independent. Firstly, since Eqs. 5 and 6 describe the same quantity, we have the first set of constraints

$$w_i - v_{c_2}/\rho = 0 \tag{9}$$

Secondly, using the rolling without slip constraints for the wheels, we have

$$R_w\dot{\Pi}_1 - v_{w_1} = 0 \tag{10}$$
$$R_w\dot{\Pi}_2 - v_{w_2} = 0 \tag{11}$$

Eqs. 9, 10, and 11 provide three constraints for each set of the castors, leading to nine kinematic constraints in total. Since these non-slippage constraints are non-holonomic, we need to use Lagrangian multipliers to formulate the equations of motion (EOM) using twelve coordinates with nine constraint equations without reducing the system to minimal order by substituting the constrained relationships.

2.3 Dynamic Control Law

For a general mechanical system with n generalized coordinates, the EOM can be formulated as

$$M(\mathbf{q})\ddot{\mathbf{q}} + N(\mathbf{q}, \dot{\mathbf{q}})\dot{\mathbf{q}} + G(\mathbf{q}) = B(\boldsymbol{q})\mathbf{u} + C^T\boldsymbol{\lambda} \tag{12}$$

We consider the case that all the kinematic constraints are not dependent on time and can be expressed as

$$C\dot{\boldsymbol{q}} = 0 \tag{13}$$

where $\mathbf{q}$ is the generalized coordinate vector, $\dot{\mathbf{q}}$ is the generalized velocity, $M(\mathbf{q})$ is a $n \times n$ symmetric, bounded, positive definite mass matrix; $N(\mathbf{q}, \dot{\mathbf{q}})\dot{\mathbf{q}}$ represents the centripetal and Coriolis torque, $G(\mathbf{q})$ is the gravity torque, $B(\boldsymbol{q})$ is the matrix that transforms the input $\mathbf{u}$ to the generalized force, C is a $m \times n$ constraint matrix, $\boldsymbol{\lambda}$ is the Lagrangian multiplier, and $C^T\boldsymbol{\lambda}$ is the constraint force. It has been proven that these kind of nonholonomic dynamic systems can not achieve asymptotical stability using smooth time-invariant state feedback [10]. The stabilization methods proposed so far include discontinuous time-invariant stabilization, time-varying stabilization, and hybrid feedback [11].

To simplify the controller for real-time application, null space formulation is used to find a solution. Choose $S(\boldsymbol{q})$ to be a $n \times (n-m)$ matrix, which is formed by a set of smooth and linearly independent vector fields spanning the null space of C, leading to

$$S^T C^T = 0 \tag{14}$$

According to Eqs. 13 and 14, since the constrained generalized velocity is always in the null space of C which is characterized by Eq. 13, a vector $\boldsymbol{v}(t) \in R^{n-m}$ can be constructed such that

$$\dot{\boldsymbol{q}} = S(q)\boldsymbol{v} \tag{15}$$

Notice that the choice of S and $\boldsymbol{v}$ is not unique. Under a certain case, $\boldsymbol{v}$ may not necessarily represent any physical velocity.

Differentiating Eq. 15, substituting it into Eq. 12, and pre-multiplying the resulted equation by S^T, we get

$$S^T M S\dot{\boldsymbol{v}} + (S^T M\dot{S} + S^T NS)\boldsymbol{v} + S^T G = S^T B\boldsymbol{u} \tag{16}$$

The new system state space equation is

$$\dot{\boldsymbol{x}} = \begin{bmatrix} S\boldsymbol{v} \\ \mathbf{0} \end{bmatrix} + \begin{bmatrix} 0 \\ I \end{bmatrix}\boldsymbol{\tau} \tag{17}$$

when the state-space vector is chosen as $\boldsymbol{x} = [\boldsymbol{q}^T, \boldsymbol{v}^T]^T$, and the control input is

$$\boldsymbol{\tau} = (S^T MS)^{-1}(S^T B\boldsymbol{u} - ((S^T M\dot{S} + S^T NS)\boldsymbol{v} + S^T G)). \tag{18}$$

Since for our 6-DOF motion emulation, the requirement for the mobile base robot is to provide a satisfactory trajectory that can extend the planar workspace of the upper high precision Stewart platform, a Lyapunov method is used to design an input-output feedback control law, which guarantees that the position and orientation errors of the mobile base are asymptotically stable and also is simpler to apply than either discontinuous or time-varying control. Accordingly, the output equation is defined as

$$\mathbf{Y} = h(\mathbf{q}) = [x; y; \psi] \tag{19}$$

Using Eq. 15, the output velocity equation is expressed as

$$\dot{\mathbf{Y}} = \frac{\partial h}{\partial \mathbf{q}} S\mathbf{v} = JS\mathbf{v} = \phi\mathbf{v} \tag{20}$$

where $J = \frac{\partial h}{\partial \mathbf{q}}$, and ϕ is the decoupling matrix of the system. The necessary and sufficient condition for the input-output linearization is that the decoupling matrix has full rank. Using symbolic manipulations, we can prove that the determinant of ϕ is -1, thus it never becomes singular. Using the Lyapunov method, we design a control law for $\boldsymbol{\tau}$ to track reference position $\mathbf{Y}_r(t)$ and reference velocity $\dot{\mathbf{Y}}_r(t)$. The Lyapunov function is defined as

$$V = 1/2(\mathbf{Y}_r - \mathbf{Y})^T K_1(\mathbf{Y}_r - \mathbf{Y}) + 1/2(\dot{\mathbf{Y}}_r - \dot{\mathbf{Y}})^T K_2(\dot{\mathbf{Y}}_r - \dot{\mathbf{Y}}) \tag{21}$$

It is easy to prove that using the control law in Eq. 22, the output tracking errors are asymptotically stable with control robustness

$$\begin{aligned} \boldsymbol{\tau} = (JS)^{-1}(\ddot{\mathbf{Y}}_r + K_1\mathbf{e} + K_2\dot{\mathbf{e}} - J\dot{S}\mathbf{v} + K_3\boldsymbol{\epsilon}) \\ \mathbf{e} = Y_r - Y \\ \dot{\mathbf{e}} = \dot{Y}_r - \dot{Y} \\ \dot{\boldsymbol{\epsilon}} = \mathbf{e} \end{aligned} \tag{22}$$

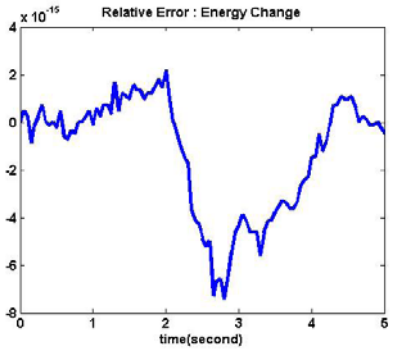

Figure 4: Energy change

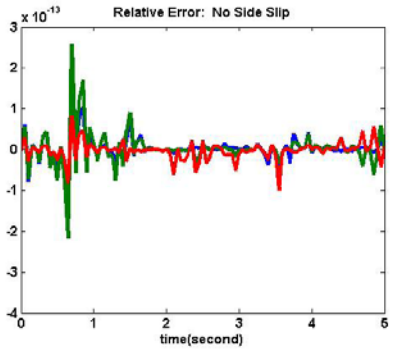

Figure 5: No side slip constraint

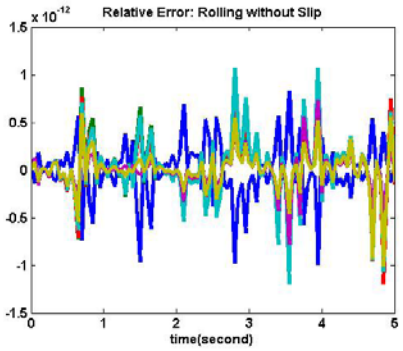

Figure 6: Rolling without slip constraint

The input torques from the six motors are solved for using Eq. 18. Notice that B is a 12×6 matrix for this redundantly controlled system. The pseudoinverse is used for the inverse of $S^T B$, yielding a minimal motor control effort.

2.4 Simulation Results

Firstly, as one of the criteria to validate the dynamic model, we numerically solve the EOM when there is no external input and then check whether the system kinematic energy remains constant or not. Theoretically, the energy should be constant. To avoid the constraint drift during integration, we utilize a constraint stabilization method which was first proposed in [12]. Dynamic response when the center of the base is doing a pure rotating motion has been validated through the simulation. The relative errors for the energy change δ_e, no side slip constraint δ_{pr} and rolling without slip constraint δ_{ns}, are calculated as the follows and are shown in Figs. 4, 5, and 6.

$$\delta_e = (E(t) - E(t_0))/E(t_0) \quad (23)$$
$$\delta_{pr} = (C_{pr}(t) - C_{pr}(t_0))/C_{pr}(t_0) \quad (24)$$
$$\delta_{ns} = (C_{ns}(t) - C_{ns}(t_0))/C_{ns}(t_0) \quad (25)$$

where $E(t)$ is the system energy at time t, $C_{pr}(t) = \dot{\theta}_1 + \dot{\psi} - v_{c_2}/\rho$ is the first castor no side slip constraint as in Eq. 9, and $C_{ns}(t) = R_w \dot{\Pi}_1 - v_{w_1}$ is the first wheel rolling without slip constraint as in Eq. 10.

Secondly, the mobile base is commanded to track a constant velocity reference trajectory with initial position and velocity errors and all the wheels are in a pulling position initially. We compare the tracking results using the dynamic controller proposed in Eq. 22 with a kinematic controller.

For the kinematic controller, knowing the reference trajectory of the mass center of the base, the top level controller generates a commanded base velocity $\boldsymbol{V}_c = \dot{\boldsymbol{Y}}_r - K(\boldsymbol{Y} - \boldsymbol{Y}_r)$, where all the symbols are defined as in Section 2.3. Through the unique mapping from the base center velocity to the wheel velocities, the kinematic controller commands the motors to track the commanded wheel velocities.

Parameters of Animatics SmartMotor 2315DT [13] are utilized in the simulation. For the dynamical controller, we achieve the commanded torque through commanding a corresponding quantized motor input voltage. The kinematic controller runs through an internal PID loop to achieve the commanded velocity.

Simulation results are shown in Figs. 7, 8, and 9. We find that both controllers can achieve satisfactory tracking while the dynamic response can be changed through tuning gains. In addition, the dynamic controller is more efficient than the kinematic controller in terms of the control efforts involved, although the dynamic controller needs more computation time than the kinematic controller. For the kinematic controller, since each wheel does not have any information about other wheels, it may fight each other during the motion. We point out that no friction models are currently implemented.

3 Overall System Simulation

Mobile manipulators have received significantly increased interest in the industrial, military, and public communities for their mobility combined with the manipulator's dexterous abilities. But most current work treats the

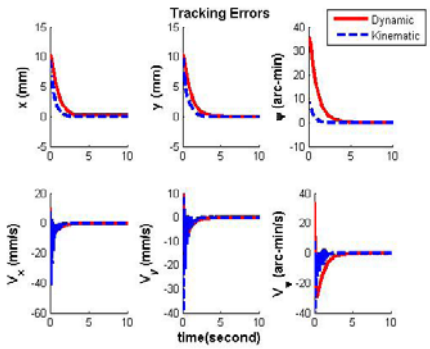

Figure 7: Tracking errors comparison

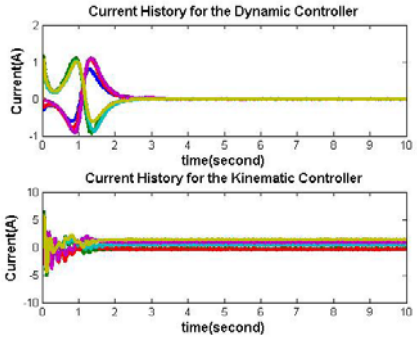

Figure 8: Current history comparison

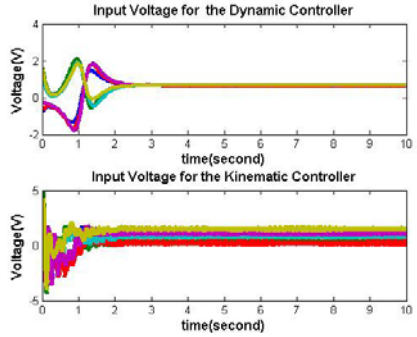

Figure 9: Voltage history comparison

system without considering dynamic interactions, only copes with holonomic constraints, or just considers the kinematic interactions [14], [15]. Since our final aim is to do a high fidelity emulation, the previous simplifications are not acceptable to us at the dynamic modeling level. We formulate a complete model of the Stewart platform and a mobile base which has non-holonomic constraints separately at first. For each subsystem, a robust controller is designed which is expected to account for the dynamic interaction forces. All the generalized coordinates are solved with the dynamic interaction forces simultaneously to solve for the true system dynamic response.

For the 6-DOF Stewart platform system, we choose the mass center location $\boldsymbol{R}_c = [X_m, Y_m, Z_m]^T$, three Euler angles $\boldsymbol{\theta}_m = [\theta_{1_m}, \theta_{2_m}, \theta_{3_m}]$ of the top plate, and the position and orientation of the base plate $\boldsymbol{q}_{b_m} = [x, y, \psi]^T$ as the generalized coordinates. We denote $\boldsymbol{q}_m = [X_m, Y_m, Z_m, \theta_{1_m}, \theta_{2_m}, \theta_{3_m}]^T$. Note that all of these coordinates are expressed with respect to the inertial frame. As we mentioned earlier, for the moving base we need to choose twelve generalized coordinates $\boldsymbol{q}_b = [x_b, y_b, \psi_b, \theta_1, \theta_2, \theta_3, \Pi_1, \Pi_2, \Pi_3, \Pi_4, \Pi_5, \Pi_6]^T$. We denote $\boldsymbol{q}_{\bar{b}} = [x_b, y_b, \psi_b]^T$ and $\boldsymbol{q}_{\bar{o}} = [\theta_1, \theta_2, \theta_3, \Pi_1, \Pi_2, \Pi_3, \Pi_4, \Pi_5, \Pi_6]^T$. Since the base plate of the Stewart platform and the triangular base of the mobile robot are rigidly connected, we assume that $\boldsymbol{q}_{\bar{b}} = \boldsymbol{q}_{b_m}$. Thus for the Stewart platform, the dynamic equations are expressed as

$$\begin{bmatrix} M_{1_m} & M_{12_m} \\ M_{12_m} & M_{2_m} \end{bmatrix} \begin{pmatrix} \ddot{\boldsymbol{q}}_m \\ \ddot{\boldsymbol{q}}_{\bar{b}} \end{pmatrix} + \begin{bmatrix} N_1 \\ N_2 \end{bmatrix} = \begin{bmatrix} Q_{1_l} \\ Q_{2_l} \end{bmatrix} + \begin{bmatrix} 0_{6\times 6} \\ Q_d \end{bmatrix} \tag{26}$$

where M_m is the mass matrix for the Stewart platform with

$$M_m = \begin{bmatrix} M_{1_m} & M_{12_m} \\ M_{12_m} & M_{2_m} \end{bmatrix} \tag{27}$$

Q_{1_l} and Q_{2_l} are the generalized forces from the Stewart platform actuator motors and projected on the generalized coordinates $\boldsymbol{q}_m$ and $\boldsymbol{q}_{\bar{b}}$, Q_d is the interaction forces/torques projected on the $\boldsymbol{q}_{\bar{b}}$ coordinates, and N_1 and N_2 are other nonlinear terms. Details about solving for the compact form of the mass matrix M can be found in [4], [5], and [16].

For the mobile moving base, the final organized dynamic equations, which have eliminated the Lagrangian multipliers by taking the derivatives of Eq. 13 and substituting Eq. 12 into them, are

$$\begin{bmatrix} M_{1_b} & M_{12_b} \\ M_{12_b} & M_{2_b} \end{bmatrix} \begin{pmatrix} \ddot{\boldsymbol{q}}_{\bar{b}} \\ \ddot{\boldsymbol{q}}_{\bar{o}} \end{pmatrix} + \begin{bmatrix} N_{1_b} \\ N_{2_b} \end{bmatrix} = \begin{bmatrix} Q_{1_b} \\ Q_{2_b} \end{bmatrix} + \begin{bmatrix} C^T(CM_b{}^{-1}C^T)^{-1}CM_b{}^{-1}Q_d \\ 0_{9\times 9} \end{bmatrix} \tag{28}$$

where M_b is the mass matrix for the mobile base

$$M_b = \begin{bmatrix} M_{1_b} & M_{12_b} \\ M_{12_b} & M_{2_b} \end{bmatrix} \tag{29}$$

$Q_{1_b} = [0, 0, 0]^T$ and $Q_{2_b} = [0, 0, 0, u_1, u_2, u_3, u_4, u_5, u_6]$ are the generalized forces from the motors; N_{1_b} and N_{2_b} are the left nonlinear terms.

Equations 26 and 28 can be reformulated as

$$M_t \begin{bmatrix} \ddot{\boldsymbol{q}}_m \\ \ddot{\boldsymbol{q}}_{\bar{b}} \\ \ddot{\boldsymbol{q}}_{\bar{o}} \\ Q_d \end{bmatrix} + \begin{bmatrix} N_1 \\ N_2 \\ N_{1_b} \\ N_{2_b} \end{bmatrix} = \begin{bmatrix} Q_{1_l} \\ Q_{1_2} \\ Q_{1_b} \\ Q_{2_b} \end{bmatrix}$$

where

$$M_t = \begin{bmatrix} M_{1_b} & M_{12_b} & 0_{6\times 9} & 0_{6\times 3} \\ M_{12_b} & M_{2_b} & 0_{3\times 9} & -I_{3\times 3} \\ 0_{9\times 6} & M_{1_b} & M_{12_b} & -C^T(CM_b{}^{-1}C^T)^{-1}CM_b{}^{-1} \\ 0_{3\times 6} & M_{12_b} & M_{2_b} & 0_{3\times 3} \end{bmatrix} \quad (30)$$

Equation 30 is the final form to use for the overall system dynamic response.

4 Conclusions and Future Work

We have presented a high fidelity dynamic model for a mobile robotic system. Complete dynamic equations of motion for each subsystem are developed and the dynamic interactions between the manipulator and the moving base are included in the system dynamic equations. The rigorous approach we undertake in this paper is indispensable to do high fidelity system analysis, control law verifications, and hardware in the loop emulation. Future work will look for a simplified dynamic controller that includes some extent of the system dynamic characteristics while needing less computation time than the current dynamic control law. We will also include the bearing frictions and scrubbing torques in the mobile base dynamic models, and combine the overall dynamic models with the sensor models and actuator models to complete the simulation.

References

[1] Jeremy Davis, James Doebbler, Kevin Daugherty, John Junkins, and John Valasek. Aerospace vehicle motion emulation using omni-directional mobile platform. South Carolina, August 2007. AIAA Guidance, Navigation, and Control (GN&C) Conference.

[2] James Doebbler, Jeremy Davis, John Valasek, and John Junkins. Mobile robotic system for ground-testing of multi-spacecraft proximity operations. Mackinac Island, Michigan, August 2007. AAS/AIAA Astrodynamics Specialist Conference.

[3] Xaioli Bai, Jeremy Davis, James Doebbler, James Turner, and John Junkins. Dynamics and Control of the Texas A& M Robotic Motion Emulation System. technial report TAMU-AERO-2007-07-26-1, Texas A&M Univeristy, College Station, TX 77843-3141, July 2007.

[4] Xiaoli Bai, James D. Turner, and John L. Junkins. Dynamic analysis and control of a stewart platform using a novel automatic differentiation method. Keystone, CO., Aug 2006. AIAA/AAS Astrodynamics Specialist Conference.

[5] Xiaoli Bai, James D. Turner, and John L. Junkins. Automatic differentiation based dynamic model for a mobile stewart platform. Greenwich, London, England, July 2006. 7th International Conference On Dynamics and Control of Systems and Structures in Space.

[6] Haoyong Yu, Matthew Spenko, and Steven Dubowsky. Omni-directional mobility using active split offset castors. *Journal of Mechanical Design*, 126(5):822–829, Sep 2004.

[7] R. Fierro and F. L. Lewis. Control of a nonholomic mobile robot: Backstepping kinematics into dynamics. *Journal of Robotic Systems*, 14(3):149 – 163, Dec 1997.

[8] Y. Kanayama, Y. Kimura, F. Miyazaki, and T. Noguchi. A stable tracking control method for an autonomous mobile robot. In *Robotics and Automation, Proc., IEEE International Conference on*, volume 1, pages 384–389, Cincinnati, OH, May 1990.

[9] Y. Yamamoto and X. Yun. Coordinating locomotion and manipulation of a mobile manipulator. In *Decision and Control, Proc. of the 31st IEEE Conference on*, volume 3, pages 2643–2648, Tucson, AZ, Dec. 1992.

[10] A.M. Bloch, M. Reyhanoglu, and N.H. McClamroch. Control and stabilization of nonholonomic dynamic systems. *Automatic Control, IEEE Transactions on*, 37(11):1746–1757, Nov 1992.

[11] I. Kolmanovsky and N.H. McClamroch. Developments in nonholonomic control problems. *Control Systems Magazine, IEEE*, 15(6):20–36, Dec. 1995.

[12] J. C. Chiou and S. D. Wu. Constraint violation stabilization using inputoutput feedback linearization in multibody dynamic analysis. *Journal of Guidance, Control, and Dynamics*, 21(2):222–228, 1998.

[13] Animatics Corporation. *Animatics SmartMotor 2315DT*. Avaliable:http://www.animatics.com.

[14] N.A.M. Hootsmans and S. Dubowsky. Large motion control of mobile manipulators including vehicle suspension characteristics. In *Robotics and Automation, Proc., IEEE International Conference on*, volume 3, pages 2336–2341, Sacramento, CA, April 1991.

[15] Jae H. Chung and Steven A. Velinsky. Robust interaction control of a mobile manipulator dynamic model based coordination. *Journal of Intelligent and Robotic Systems*, 26(1):47–63, Sep 1999.

[16] Hanspeter. Schaub and John L. Junkins. *Analytical Mechanics of Space Systems*. AIAA, 2003.